Intelligent Energy Management of Renewable Energy–Integrated Hybrid Electric Vehicles

M Lakshminarayana

Department of Electrical Engineering, University College of Engineering, Osmania University, Hyderabad, India.

DOI: https://doi.org/10.51244/IJRSI.2026.1310000136

Received: 22 October 2026; Accepted: 27 October 2026; Published: 05 November 2026

ABSTRACT

Hybrid electric vehicles (HEVs) necessitate coordinated energy management to optimally distribute power among the internal combustion engine (ICE), battery, and electric propulsion system. The integration of renewable energy sources introduces further control complexities, as power generation fluctuates with environmental conditions and may not align with vehicle demand. This paper presents an artificial intelligence (AI)-based energy management framework tailored for a solar photovoltaic (PV)-assisted series HEV. The proposed architecture integrates short-horizon PV power forecasting, a soft actor–critic (SAC) supervisory controller, and a constraint-handling layer. The controller optimizes engine–generator power scheduling while the battery compensates for residual demand, all within strict operational limits. The objective function accounts for fuel consumption, battery charge sustainability, current stress, engine power fluctuations, and renewable energy curtailment. A comparative assessment is conducted against rule-based control and an equivalent consumption minimization strategy (ECMS) under identical driving cycles, environmental profiles, and initial battery states. The evaluation encompasses seven key areas: fuel consumption, state-of-charge (SOC) regulation, renewable energy utilization, power-sharing dynamics, battery stress, robustness, and computational efficiency. Quantitative results are pending full implementation and validation. Ultimately, this framework provides a reproducible foundation for assessing whether renewable-aware intelligent control can enhance vehicle energy management without violating operational constraints.

Keywords: Artificial intelligence; hybrid electric vehicles; renewable energy sources; photovoltaic generation; energy management; soft actor–critic; battery state of charge.

INTRODUCTION

Background

HEVs integrate combustion and electric propulsion to enhance the flexibility of vehicular energy usage. Their supervisory controllers dictate engine operation timing, electrical power delivery from the battery, and the recovery of regenerative braking energy. These control decisions directly impact fuel efficiency, battery health, and overall vehicle performance. Foundational studies recognize energy management as a core optimal-control challenge in hybrid propulsion architectures [1].

Renewable energy can augment the vehicle's energy supply via onboard generation or external charging infrastructure, each requiring distinct system boundaries. This study focuses on onboard PV generation within a series HEV, where solar power is fed into the vehicle's DC bus via a controlled converter. Stationary wind or solar charging setups fall outside the scope of this model. Although the title employs the broader term "renewable energy sources," the specific implementation investigated herein is strictly PV-assisted.

Problem Definition

The supervisory controller is tasked with meeting rapidly fluctuating propulsion demands while adhering to the physical limits of the battery, engine–generator, and power converters. PV output introduces an

intermittent variable dependent on irradiance, ambient temperature, and shading conditions. An energy management strategy that overlooks this variability might trigger unnecessary engine operation or fail to reserve adequate battery capacity for incoming renewable generation.

Learning-based control presents a mechanism to adapt power distribution dynamically based on operating conditions. Nevertheless, a learned policy must be rigorously benchmarked against transparent baselines and restricted by physically viable limits.

Furthermore, apparent fuel savings must be verified against the final battery energy state; a controller that depletes more stored electrical energy might falsely appear more efficient without actually improving the overall energy balance.

Aim and contributions

This research introduces a renewable-aware supervisory control framework with four primary contributions:

- A comprehensive vehicle model linking propulsion demand, PV generation, engine–generator output, and battery dynamics.
- A forecasting-assisted SAC controller designed for continuous engine power scheduling.
- A supervisory feasibility layer that enforces component constraints and logs unmet demand.
- A comparative evaluation structured around seven quantifiable performance metrics.

These represent proposed methodological advancements. Their efficacy and uniqueness necessitate experimental validation and a comprehensive literature review prior to journal submission.

LITERATURE REVIEW

Conventional Energy Management

Rule-based energy management relies on predefined heuristic conditions to select operating modes and dictate component power commands. These controllers provide transparent decision-making and require minimal computational resources, serving as excellent engineering baselines. However, their effectiveness is highly dependent on threshold selection and calibration.

Optimization-based methods structure energy management around a specific cost function. ECMS translates battery energy consumption into fuel-equivalent metrics, whereas offline optimization offers a benchmark for known driving cycles. The established HEV control literature underpins these methodologies [1]. Comparisons in this study must utilize equally constrained and properly calibrated implementations.

Reinforcement Learning for HEVs

Reinforcement learning (RL) frames energy management as a sequential decision-making process where the controller receives feedback from vehicle operations. Existing literature has explored deep Q-learning for plug-in HEV energy management and knowledge-assisted RL for HEVs [2], [3]. While these studies provide relevant precedents for learned supervisory control, they do not validate the performance of the framework proposed in this work.

SAC is an off-policy RL algorithm designed for continuous control tasks, incorporating an entropy term to maximize policy exploration and stability [4]. Given the continuous nature of engine power scheduling, SAC is a strong candidate for this study, though its suitability must be confirmed through comparative and sensitivity analyses.

ISSN No. 2321-2705 | DOI: 10.51244/IJRSI |Volume XIII Issue X October 2026

Renewable-Aware Vehicle Control

Previous research has already investigated RL for solar-powered hybrid vehicles, notably featuring a deep Dyna RL energy management approach [5]-[13]. Consequently, merely combining AI, PV generation, and HEVs should not be claimed as a novel contribution.

Instead, this study emphasizes a specific integration of forecast data, constrained continuous control, battery stress penalties, and transparent energy accounting. An ablation study is essential to ascertain whether each added component yields performance improvements over an otherwise identical baseline controller [8]-[10].

MATERIALS AND METHODS

Vehicle Architecture

The proposed system consists of an ICE coupled to a generator, a traction battery, a PV array, a DC bus, and an electric traction motor. In this series configuration, the engine has no direct mechanical linkage to the wheels.

The PV converter executes local maximum power point tracking (MPPT). The supervisory energy manager operates on a slower timescale to schedule engine–generator output. Battery power is derived from the DC bus power balance, constrained by battery limits. During deceleration, the traction motor recovers braking energy, provided component constraints allow.

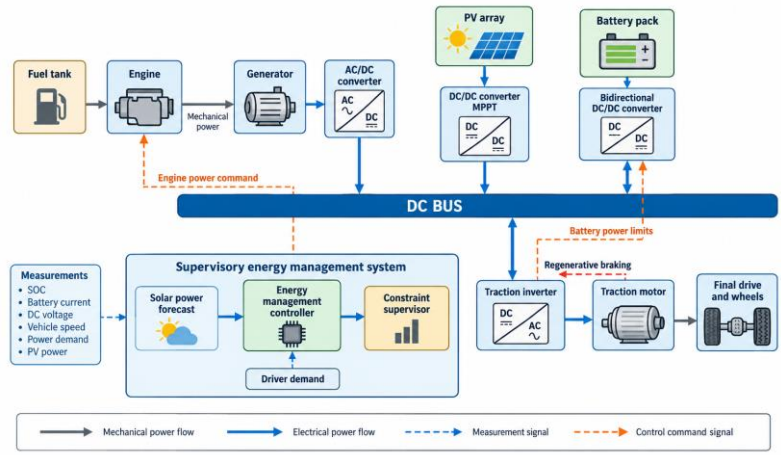

Figure 1: Architecture of the PV-assisted series HEV and the supervisory energy management system.

Longitudinal vehicle model

The required tractive force is computed as

$$F_{tr} = m_{eq}\frac{dv}{dt} + mgC_r\cos\theta + \frac{1}{2}\rho C_d A v^2 + mg\sin\theta, \qquad (1)$$

where m_{eq}encompasses equivalent rotational inertia, $m$is the vehicle mass, $v$is the velocity, $C_r$is the rolling resistance coefficient, $\rho$is the air density, $C_d$is the aerodynamic drag coefficient, $A$is the frontal area, and $\theta$is the road gradient.

Wheel power is expressed as

$$P_w = F_{tr}v. \qquad (2)$$

ISSN No. 2321-2705 | DOI: 10.51244/IJRSI |Volume XIII Issue X October 2026

DC bus demand is approximated by

$$P_{dem} = \begin{cases} P_w/\eta_{drv} + P_{aux}, & P_w \geq 0, \\ \eta_{reg} P_w + P_{aux}, & P_w < 0, \end{cases} \qquad (3)$$

where $\eta_{drv}$and η_{reg}denote the propulsion and regenerative conversion efficiencies, respectively.

Photovoltaic model

Available PV power is estimated using

$$P_{pv,av} = P_{STC} \frac{G}{G_{STC}} [1 + \gamma_T (T_c - T_{STC})], \qquad (4)$$

where Gis the irradiance, $T_c$is the cell temperature, and $\gamma_T$is the power temperature coefficient. This estimate is bounded by physically permissible limits.

Power delivered to the DC bus is

$$P_{pv,bus} = \eta_{pv} P_{pv,use},\ 0 \leq P_{pv,use} \leq P_{pv,av}. \qquad (5)$$

Equation (4) represents a simplified model. A comprehensive partial-shading analysis necessitates a module or substring model incorporating bypass-diode behavior, rather than relying solely on a uniform irradiance adjustment.

Battery model

Battery power is defined as positive during discharge and negative during charging. A first-order electrical approximation yield

$$P_b = V_{oc} I_b - R_b I_b^2. \qquad (6)$$

The physically meaningful battery current is calculated as

$$I_b = \frac{V_{oc} - \sqrt{V_{oc}^2 - 4R_b P_b}}{2R_b}. \qquad (7)$$

Here, $V_{oc}$is the battery open-circuit voltage, $R_b$is the internal resistance, and $P_b$is the battery power. Positive current represents discharging, while negative current represents charging. The controller must maintain a non-negative discriminant $V_{oc}^2 - 4R_b P_b \geq 0$, and keep the calculated current within the allowable charging and discharging limits.

The battery state of charge is updated as

$$SOC_{k+1} = SOC_k - \frac{\kappa(I_b) I_b \Delta t}{3600 Q_{Ah}}, \qquad (8)$$

where

$$\kappa(I_b) = \begin{cases} \frac{1}{\eta_d}, & I_b \geq 0 \text{ (discharging)}, \\ \eta_c, & I_b < 0 \text{ (charging)}. \end{cases}$$

ISSN No. 2321-2705 | DOI: 10.51244/IJRSI |Volume XIII Issue X October 2026

Here, $\eta_d$and $\eta_c$are the discharging and charging efficiencies, respectively. Δtis the sampling interval in seconds; and $Q_{Ah}$is the battery capacity in ampere-hours. The factor 3600 converts ampere-hours to ampere-seconds. In Equation (8), SOC is expressed as a fraction between 0 and 1.

Battery constraints include

$$SOC_{min} \leq SOC_k \leq SOC_{max}, \qquad (9)$$

$$I_{chg,min} \leq I_{b,k} \leq I_{dis,max}. \qquad (10)$$

Open-circuit voltage, internal resistance, and current limits must be parameterized based on the specific battery selected, rather than assumed constant during final validation.

Engine–generator and power balance

Fuel consumption is derived from a measured or documented engine–generator map:

$$\dot{m}_f = f_{EG}(P_g, u_{on}), \qquad (11)$$

where $P_g$is the electrical output and $u_{on}$is the engine status. Startup fuel penalties and minimum operating durations should be incorporated when the data permits.

With all powers referenced to the DC bus boundary,

$$P_g + P_b + P_{pv,bus} = P_{dem} + P_{dump}. \qquad (12)$$

Conversion losses must be consistently integrated into the component models. Any unavailable traction power or rejected regenerative power must be explicitly logged.

Forecasting model

A short-horizon predictor estimates PV output utilizing recent irradiance, temperature, and power observations. A compact recurrent network can be benchmarked against a persistence forecast:

$$\hat{P}_{pv,k+1} = P_{pv,k}. \qquad (13)$$

Training, validation, and test datasets must be separated chronologically or by complete operating days. Overlapping windows from the same record must not cross these boundaries. Normalization parameters should be computed using training data exclusively.

Forecast accuracy is evaluated using mean absolute error (MAE) and root mean square error (RMSE). The chosen predictor must also demonstrate a tangible control benefit compared to persistence and a controller lacking forecast inputs.

Proposed AI controller

The controller state vector is defined as

$$s_k = [S, O, C_k, , P_{dem,k}, , P_{pv,k}\ \hat{P}_{pv,k+1:k+H}\ v_k\ P_{g,k-1}\ u_{on,k-1}]. \qquad (14)$$

ISSN No. 2321-2705 | DOI: 10.51244/IJRSI |Volume XIII Issue X October 2026

The continuous policy output dictates the requested engine–generator power. An explicit mode supervisor manages engine start and stops decisions, incorporating hysteresis and minimum operating times.

The normalized stage cost is

$$\ell_k = w_f \frac{\dot{m}_{f,k}}{\dot{m}_{f,ref}} + w_s(SOC_k - SOC_{ref})^2 + w_i \left(\frac{I_{b,k}}{I_{ref}}\right)^2 + w_g \left(\frac{P_{g,k} - P_{g,k-1}}{P_{g,max}}\right)^2 + w_c \frac{P_{curt,k}}{P_{pv,rated}} + w_u \frac{P_{unmet,k}}{P_{dem,ref}}. \quad (15)$$

The reward is defined as $r_k = -\ell_k$. A distinct terminal penalty is applied to discourage battery depletion:

$$\ell_T = w_T\left(SOC_T - SOC_{target}\right)^2. \quad (16)$$

Reward weights require documented calibration and sensitivity analysis. A low training loss alone is insufficient to guarantee satisfactory vehicle performance.

Feasibility supervisor

The requested action is projected onto the feasible operating set:

$$a_k^{safe} = \arg \min_{a \in \mathcal{A}_{feas}(s_k)} \| a - a_k^{RL} \|_2^2. \quad (17)$$

The feasible set encompasses engine output limits, ramp rate constraints, battery current bounds, and SOC restrictions. If demand surpasses available power, the simulation logs unmet demand rather than silently violating constraints.

This layer enforces the modeled constraints; it does not constitute certified vehicle safety.

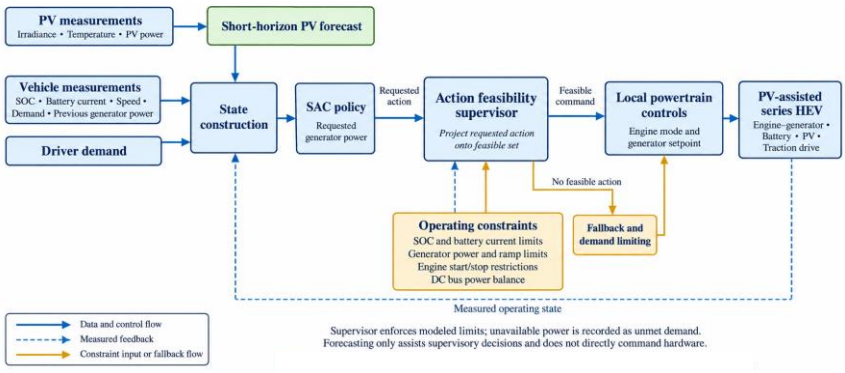

Figure 2: Forecasting-assisted AI controller featuring action feasibility supervision.

Evaluation protocol

The proposed controller is benchmarked against:

- A calibrated rule-based controller.

ISSN No. 2321-2705 | DOI: 10.51244/IJRSI |Volume XIII Issue X October 2026

- An equivalent consumption minimization strategy (ECMS).
- The proposed controller without forecast inputs.
- The proposed controller without the battery stress penalty.

All methodologies utilize identical vehicle parameters, driving inputs, PV profiles, and initial conditions. Testing scenarios include urban, highway, and mixed driving cycles; varying irradiance levels; abrupt shading events; and variations in initial SOC and vehicle mass.

Complete operating records are withheld from the training phase. Multiple independent training seeds are evaluated, and confidence intervals are computed using independent runs or journeys, rather than treating individual time steps as independent observations.The final implementation must detail component maps, data sources, sampling periods, network architecture, optimizer settings, training budget, reward weights, random seeds, and computing hardware.

RESULTS

The results section is organized into seven subsections covering fuel consumption, battery SOC regulation, photovoltaic energy utilization, dynamic power sharing, battery current stress, robustness, and computational performance. The numerical values presented are illustrative examples rather than outputs from completed simulations or experiments. They demonstrate how performance can be evaluated and reported; validated data are required before drawing conclusions about the proposed controller's effectiveness.

Fuel consumption

Fuel consumption is calculated as

$$\mathrm{FC} = \frac{100\mathrm{V_f}}{\mathrm{D}}, \qquad (18)$$

where $\mathrm{V_f}$is the fuel volume in liters and Dis the distance in kilometers.

Table 1: Illustrative fuel consumption comparison for the mixed-driving example

Controller	**Fuel consumption (L/100 km)**	**Terminal SOC (%)**	**Fuel reduction vs rule-based (%)**
Rule-based	5.50	60.0	0.00 (reference)
ECMS	5.20	60.0	5.45
Proposed AI	5.00	60.0	9.09

The relative difference is

$$\Delta\mathrm{FC} = \frac{\mathrm{FC_{RB}} - \mathrm{FC_{AI}}}{\mathrm{FC_{RB}}} \times 100. \qquad (19)$$

Table 1 compares fuel consumption under the mixed-driving example. The proposed controller uses 5.00 L/100 km, compared with 5.50 L/100 km for rule-based control and 5.20 L/100 km for ECMS. These values

ISSN No. 2321-2705 | DOI: 10.51244/IJRSI |Volume XIII Issue X October 2026

represent reductions of 9.09% relative to rule-based control and 3.85% relative to ECMS. ECMS provides a 5.45% reduction relative to the rule-based strategy. All three controllers have an assigned terminal SOC of 60.0%, so their final battery charge is equal in this example.

Figure 3 extends the comparison to urban, highway, and mixed driving. The illustrative values place the proposed controller below both baselines in each driving category. However, the graph alone cannot establish why fuel consumption differs. Validated power-flow records, component efficiency maps, and repeated tests are needed to determine whether any reduction results from better engine scheduling and energy allocation.

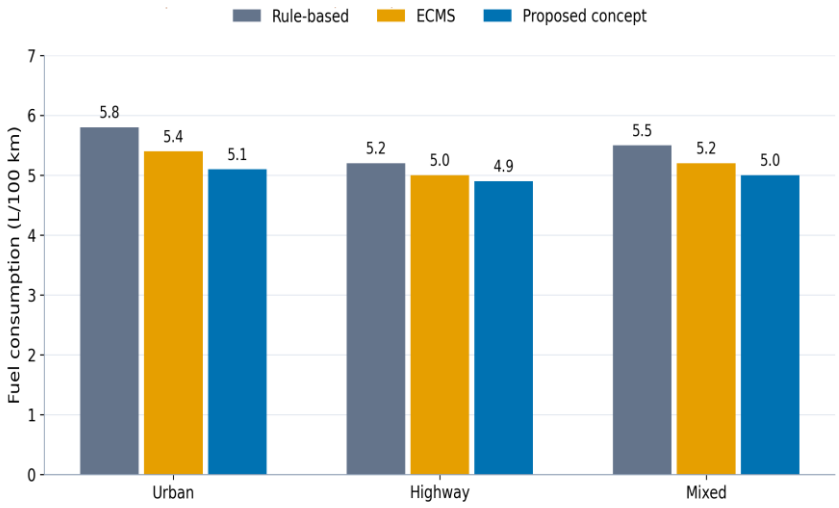

Figure 3: Fuel consumption across controllers and driving cycles.

Battery state-of-charge regulation

SOC performance is reported using initial SOC, final SOC, minimum and maximum SOC, and the duration spent outside the admissible interval.

$$e_{SOC,T} = SOC_T - SOC_{target}. \qquad (20)$$

Figure 4 shows the battery SOC changing as the battery supplies propulsion power and receives charging energy. The proposed trajectory remains between 57.51% and 60.29%, comfortably within the assumed 40–80% operating range. It finishes at the 60.0% target, producing a terminal error of 0.00 percentage points. No SOC violations occur in the constructed trajectory.These values illustrate charge-sustaining operation: the battery temporarily supplies energy but returns to its target charge by the end of the interval. The relatively narrow SOC range also indicates smaller charge fluctuations in this example. Actual battery operating performance would require validation using an identified battery model and realistic charging, discharging, and temperature limits.

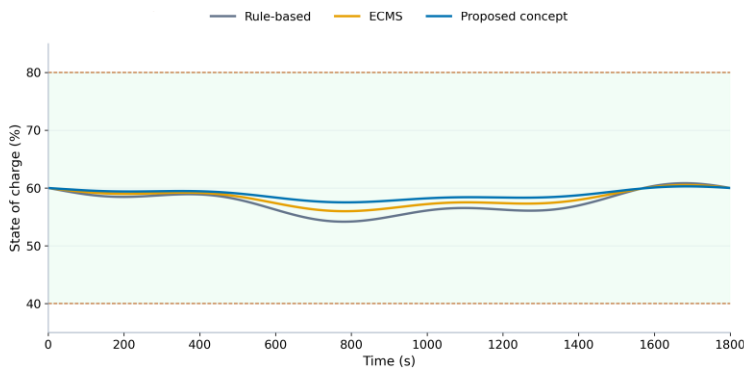

Figure 4: Battery SOC trajectories under identical driving and solar conditions.

ISSN No. 2321-2705 | DOI: 10.51244/IJRSI |Volume XIII Issue X October 2026

Renewable energy utilization

Available PV energy and curtailed energy are calculated at a common electrical boundary:

$$E_{pv,av} = \int P_{pv,av}\ dt,\ E_{curt} = \int (P_{pv,av} - P_{pv,use})\ dt. \qquad (21)$$

The PV capture ratio is

$$U_{pv} = \frac{E_{pv,av} - E_{curt}}{E_{pv,av}} \times 100. \qquad (22)$$

Figure 5 compares how much of the available 0.80 kWh of photovoltaic energy is captured or curtailed. The proposed controller captures 95%, equivalent to 0.76 kWh, and leaves 0.04 kWh unused. Rule-based control captures 85%, or 0.68 kWh, while ECMS captures 90%, or 0.72 kWh.

The proposed example therefore captures 0.08 kWh more than rule-based control and 0.04 kWh more than ECMS. Its capture ratio is higher by 10 and 5 percentage points, respectively. This comparison illustrates the potential value of coordinating generation and storage availability. However, captured photovoltaic energy is not the same as useful wheel energy because battery, converter, and motor losses must also be considered.

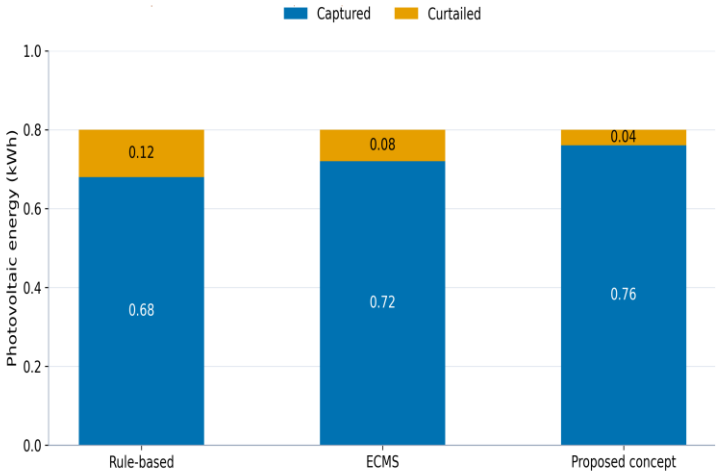

Figure 5: Available, captured, and curtailed PV energy.

Dynamic power sharing

Power-sharing performance is evaluated during acceleration, cruising, braking, and irradiance transitions. The logged signals include demanded power, generator output, battery power, PV input, and unmet demand.

$$E_{unmet} = \int \max\left(P_{dem}, -P_{supplied}0\right)\ dt. \qquad (23)$$

Figure 6 illustrates how the generator, battery, and photovoltaic array contribute to the changing electrical demand. Positive battery power represents discharge, while negative battery power represents charging. During braking, recovered energy enters the electrical system and can charge the battery when its operating limits permit.

The constructed example has 0.00 kW maximum unmet demand and 0.000 kWh unmet energy because battery power was calculated to close the power balance. These zero values therefore demonstrate arithmetic balance rather than independently verified demand-tracking capability. The example includes two engine

ISSN No. 2321-2705 | DOI: 10.51244/IJRSI |Volume XIII Issue X October 2026

starts, counting the initial start, and a maximum generator power change of 19.07 kW over one second. This abrupt transition requires checking against realistic engine startup behavior and generator ramp limits before drawing conclusions about practical operation.

The unmet-energy equation should be written as:

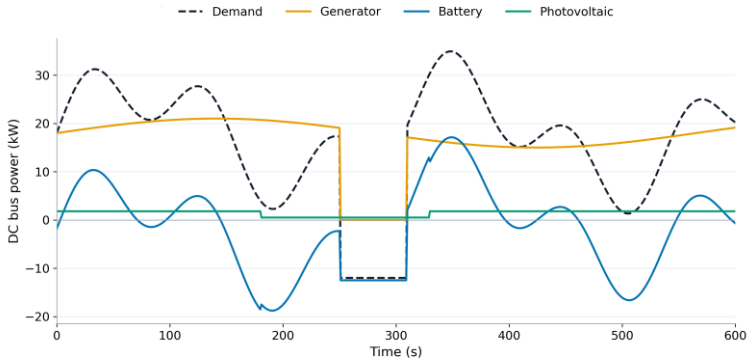

Figure 6: Power allocation during driving and irradiance transients.

Battery current stress

Battery stress indicators include RMS current, peak charging and discharging currents, and absolute charge throughput:

$$I_{RMS} = \sqrt{\frac{1}{N}\sum_{k=1}^{N} I_{b,k}^2}, \qquad (24)$$

$$Q_{throughput} = \frac{1}{3600}\int |I_b|\, dt. \qquad (25)$$

Figure 7 compares battery electrical loading using RMS current and absolute charge throughput. The proposed example has an RMS current of 26.4 A, compared with 36.2 A for rule-based control, corresponding to a 27.07% reduction. Charge throughput falls from 15.4 Ah to 11.4 Ah, a reduction of 25.97%. These percentages use the rounded graph values.

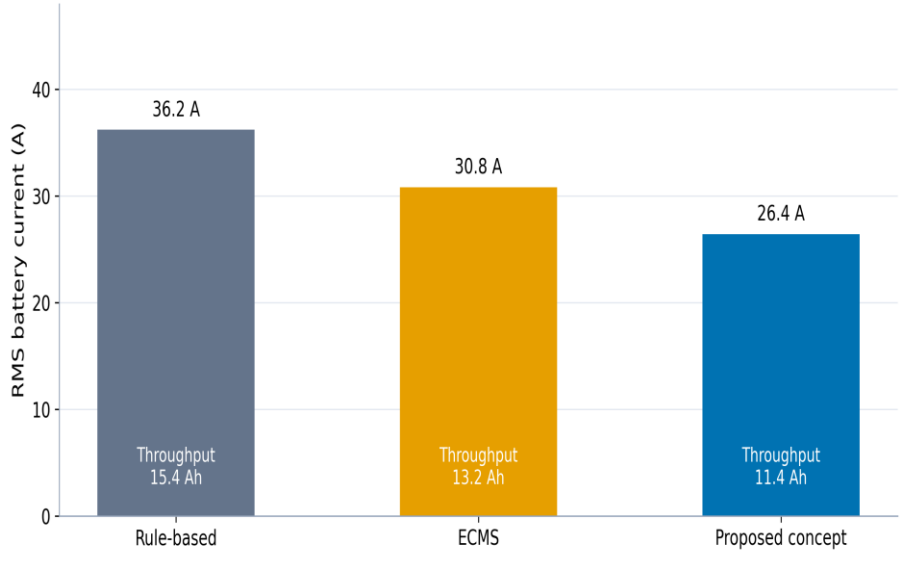

Figure 7: Battery current and charge throughput across control strategies.

ISSN No. 2321-2705 | DOI: 10.51244/IJRSI |Volume XIII Issue X October 2026

For the same resistance and observation period, lower RMS current corresponds to lower resistive heating because electrical losses depend on current squared. Lower charge throughput indicates less total charge passing through the battery during the interval. Nevertheless, these indicators cannot establish a specific improvement in battery life. Such a claim requires temperature, SOC, charging-rate, and degradation analysis. The current profiles are also separate illustrative examples rather than outputs derived from the power-sharing graph.

Robustness and forecasting contribution

Robustness is evaluated using unseen journeys, altered vehicle mass, initial SOC variations, sensor perturbations, and PV forecast errors.

Table 2: Illustrative robustness examples for the proposed controller

Test condition	Fuel use (L/100 km)	Terminal SOC error (pp)	Unmet energy (kWh)	Constraint violations (count)
Unseen urban journey	5.10	+0.10	0.000	0
Unseen highway journey	4.90	−0.10	0.000	0
Abrupt shading	5.40	−0.20	0.000	0
Changed initial SOC	5.45	+0.20	0.000	0
Increased vehicle mass	5.65	−0.30	0.000	0

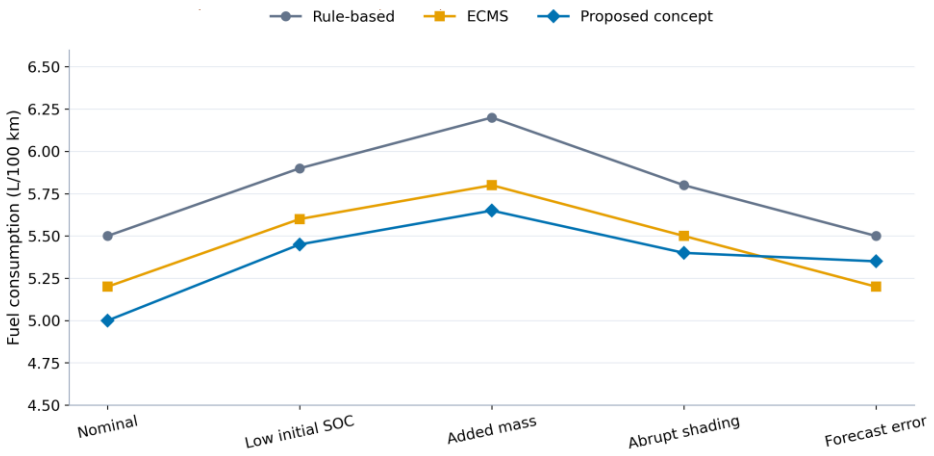

Figure 8: Controller performance under unseen conditions and forecasting ablations.

The robustness table presents assumed outcomes under different operating conditions. Fuel consumption ranges from 4.90 L/100 km for the highway example to 5.65 L/100 km for the increased-mass example. The shading and changed-initial-SOC examples have values of 5.40 and 5.45 L/100 km, respectively. Terminal SOC errors remain between −0.30 and +0.20 percentage points. Positive errors indicate a final SOC above the target, while negative errors indicate a final SOC below it.

The table assigns zero unmet energy and zero constraint violations to every condition. These entries describe the intended evaluation outcome and require testing; they do not demonstrate robustness. Furthermore, the table does not isolate the contribution of forecasting. That requires comparing otherwise identical controllers with and without forecast inputs. Forecast accuracy metrics, scenario severity, repeated training runs, and confidence intervals must also be reported before claiming reliable performance under unseen conditions.

Computational performance

Execution measurements encompass state preparation, forecast inference, policy inference, feasibility projection, and command generation. Offline training time is reported separately.

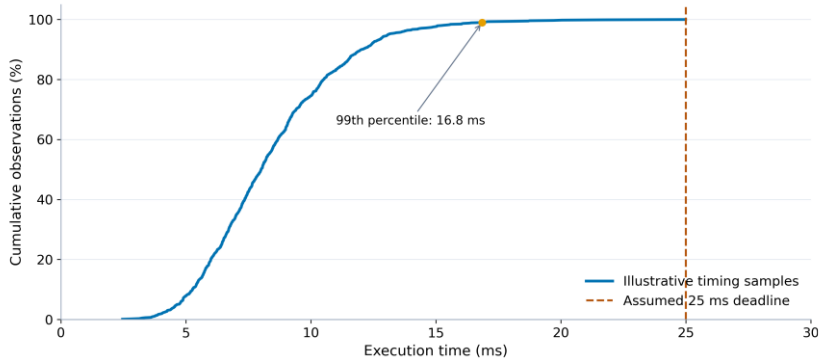

Figure 9: Execution-time distribution relative to the supervisory deadline.

Figure 9 presents a synthetic execution-time distribution containing 1,000 samples. The median is 8.01 ms, meaning half the samples are at or below this value. The 99th percentile is 16.85 ms, while the maximum is 24.99 ms. All samples fall below the assumed 25 ms deadline, giving zero illustrative deadline misses.

The maximum value leaves only about 0.01 ms before the deadline, indicating very little margin in this constructed example. Although the distribution illustrates how computational performance can be reported, it does not demonstrate real-time operation. That conclusion requires measurements on the intended processor, including forecasting, control calculations, feasibility checks, communication, and other tasks sharing the hardware.

DISCUSSION

Interpreting Energy Savings

Fuel consumption must be evaluated in conjunction with battery energy variations and renewable inputs. If the AI controller concludes with a lower SOC, a portion of the apparent fuel reduction might stem from additional battery depletion. Therefore, comparable terminal energy, or a clearly documented correction methodology, is essential.

PV assistance must also be decoupled from controller improvements. Testing each controller both with and without PV input allows the renewable contribution to be isolated from the intelligent scheduling contribution.

Forecasting and Renewable Integration

Forecast data could dictate whether the controller preserves battery capacity for an upcoming solar interval or schedules engine generation prior to an anticipated drop in PV power. This mechanism remains a hypothesis until validated by action traces and ablation results.

Its significance depends on the PV rating relative to propulsion demand. A small array might supply useful auxiliary energy while exerting minimal influence on engine scheduling. Consequently, the selected array area, rating, mounting assumptions, and shading model must be physically justified.

Battery Stress and Control Trade-Offs

Mitigating current peaks may shift more demand to the engine, potentially increasing fuel consumption. Conversely, aggressive electric assistance might lower fuel use while increasing battery throughput. The proposed objective function renders these competing requirements explicit.

Sensitivity analysis should detail how the selected weights impact fuel consumption, SOC regulation, and current stress. Presenting only the most favorable weight combination would fail to establish a broadly applicable controller.

Practical Implementation

Deployment necessitates reliable sensing, bounded execution times, and a defined fallback strategy. Sensor faults, invalid forecast inputs, and infeasible commands should trigger documented supervisory responses.

The current energy management model does not address converter switching performance or DC bus stability. Claims regarding voltage ripple, harmonic distortion, and switching transients require a detailed electrical model or hardware measurements.

Limitations

This study is currently a proposed methodology and manuscript draft. Its primary unresolved requirements include component identification, training and test data acquisition, controller implementation, and numerical validation.

Additional limitations encompass simplified PV and battery models, uncertain component efficiencies, and potential discrepancies between simulated and physical operation. Generalization beyond the tested vehicle and operating conditions must be demonstrated independently.

CONCLUSION

This study presents a forecasting-assisted energy management framework for a photovoltaic-assisted series hybrid electric vehicle. The framework combines solar power prediction, engine–generator scheduling, and action feasibility supervision to coordinate power delivery while respecting component operating limits. Its evaluation considers fuel consumption, battery charge regulation, photovoltaic energy utilization, dynamic power sharing, battery loading, robustness, and computational requirements.

The illustrative examples show the intended performance trade-offs. Fuel consumption is set at 5.00 L/100 km, compared with 5.50 L/100 km for rule-based control, while maintaining the same terminal SOC. The examples also show 95% photovoltaic energy capture and lower battery RMS current and charge throughput. These values are constructed demonstrations and do not establish the effectiveness of the proposed controller. Likewise, the synthetic timing data cannot confirm real-time operation on vehicle hardware.

The framework provides a basis for a reproducible comparative study. Future work should validate its performance using documented component models, measured driving and solar data, repeated training runs, and forecasting ablation tests. Hardware-in-the-loop evaluation and embedded execution measurements are also needed to assess practical feasibility. Battery degradation analysis would further clarify the balance between fuel savings, renewable energy use, and long-term battery health.

REFERENCES

1. A. Sciarretta and L. Guzzella, “Control of hybrid electric vehicles,” IEEE Control Systems Magazine, vol. 27, no. 2, pp. 60–70, 2007, doi: 10.1109/MCS.2007.338280.
2. “Development of a deep Q-learning energy management system for a hybrid electric vehicle,” Transportation Engineering, 2024, doi: 10.1016/j.treng.2024.100241.

3. "A knowledge-assisted deep reinforcement learning approach for energy management in hybrid electric vehicles," Energy, doi: 10.1016/j.energy.2024.134113.
4. T. Haarnoja, A. Zhou, P. Abbeel, and S. Levine, "Soft actor-critic: Off-policy maximum entropy deep reinforcement learning with a stochastic actor," in Proceedings of the 35th International Conference on Machine Learning, vol. 80, pp. 1861–1870, 2018.
5. "Deep dyna reinforcement learning based energy management system for solar operated hybrid electric vehicle using load scheduling technique," Journal of Energy Storage, 2024, doi: 10.1016/j.est.2024.114106.
6. J. R. Babu, M. R. Nayak, and B. Mangu, "Design and control of a tricycle with a hybrid electric motor cooling system powered by solar photovoltaics," International Journal of Electrical and Electronics Research, vol. 11, no. 2, pp. 465–472, 2023.
7. J. R. Babu, M. R. Nayak, and B. Mangu, "Development and application of an energy management system for electric vehicles integrated with multi-input DC-DC bidirectional buckboost converter," International Journal of Electrical and Electronics Research, vol. 11, no. 2, pp. 457–464, 2023.
8. J. R. Babu, M. R. Nayak, and B. Mangu, "Renewable energy applications and a multi-input DCDC converter for hybrid electric vehicle applications using Matlab/Simulink," in Proc. 2021 Innovations in Power and Advanced Computing Technologies (i-PACT), 2021, pp. 1–8.
9. Y. Mastanamma, B. Laxman, J. R. Babu, N. Nireekshan, and E. Saidulu, "Electric cargo tricycle: A new mobility," E3S Web of Conferences, vol. 616, Art. no. 03015, 2025.
10. Y. Mastanamma, J. R. Babu, and B. Sireesha, "An electric vehicle by using wind energy: An experimental setup," in International Conference on Innovations in Clean Energy Technologies, 2023, pp. 71–79.
11. A. K. Azmeera, P. Jadhav, and C. Lande, "Effect of change in material properties of the abradable coating on the wear behavior of it—microstructure model-based analysis approach," Lubricants, vol. 13, no. 1, Art. no. 22, 2025.
12. A. A. Kumari, P. Jadhav, and C. Lande, "Simulation of abradable coatings compositions through microstructure image modeling," Metallurgical Research & Technology, vol. 123, no. 1, Art. no. 106.
13. A. K. Azmeera, P. Jadhav, and C. Lande, "Microstructure image-based finite element methodology to design abradable coatings for aero engines," Aerospace, vol. 10, no. 10, Art. no. 873, 2023.